Co-doped LaAlO3 perovskite oxide for NOx-assisted soot oxidation

Quang Nguyen Tran, Ferenc Martinovic, Monica Ceretti, Serena Esposito, Barbara Bonelli, Werner Paulus, Francesco Di Renzo, Fabio Deorsola, Samir Bensaid, Raffaele Pirone

Co-doped LaAlO3 perovskite oxide for NOx-assisted soot oxidation

Quang Nguyen Tran[a,b], Ferenc Martinovic[a], Monica Ceretti[b], Serena Esposito[a], Barbara Bonelli[a], Werner Paulus[b], Francesco Di Renzo[b], Fabio A. Deorsola[a],*, Samir Bensaid$_a$, Raffaele Pirone[a]

a Department of Applied Science and Technology, Politecnico di Torino, Corso Duca degli Abruzzi, 24, 10129 Torino, Italy

b Institut Charles Gerhardt, Université de Montpellier-CNRS-ENSCM, Place Eugène Bataillon, 34095 Montpellier Cedex 5, France

Keywords: Soot; Oxidation; NOx-assistance; Perovskite; NOx storage; Oxygen mobility

Supplementary material: doi:https://doi.org/10.1016/j.apcata.2019.117304.

Abstract

In the framework of nowadays challenges in the automotive catalysis, directed to the mitigation of pollution caused by the emissions of internal combustion engines, a series of LaAl1-xCoxO3 perovskites were investigated with the purpose of enhancing the oxidation of soot in the presence of NOx. Perovskite oxides LaAl1-xCoxO3 (x=0; 0.25; 0.5; 0.75 and 1) were synthesized by a sol-gel route and characterized by different methods: X-Ray diffraction (XRD), H2-temperature programmed reduction (H2-TPR), N2-sorption, O2/NOx-temperature programmed desorption (TPD) and X-ray photoelectron spectroscopy (XPS). The perovskite oxides were tested as catalysts for NO oxidation in isothermal mode and for NOx-assisted soot oxidation in temperature programmed reaction. Structural results reveal that Co is well incorporated in the perovskite structure expanding the unit cell, and doping Co may result in the distortion of the BO6 octahedra of the general ABO3 perovskite structure. An increase in Co substitution with x up to 0.75 remarkably promotes the oxidation activity, whereas total replacement of Al by Co degrades the catalytic performance. Among the prepared solids, LaAl0.25Co0.75O3 is the most active for NO oxidation, with a conversion of 78% at 320 °C, and it also exhibits the highest activity for NOx-assisted soot oxidation, with a T10% of 377 °C while maintaining high NO2 production (71%). The outstanding performance of LaAl0.25Co0.75O3 is associated with the high mobility of lattice oxygen species and the role of surface adsorbed oxygen seems not to be prominent. The strong correlation of catalytic activity with NOx-TPD profiles suggests that NOx adsorption on catalyst surface is an essential step in soot oxidation. It is also shown that higher calcination temperature promotes the crystallinity of perovskite phase and leads to the improvement in the catalytic activity. The present work indicates that the prepared perovskite catalysts are competitive with noble-metal rivals for NOx-assisted soot oxidation and outperform them in NO2 production for further NOx abatement.

1. Introduction

Perovskite oxides have general formula ABO3, where the 12-fold cubo-octahedral A site is usually occupied by alkaline earth/alkaline or larger cations and the octahedral B-site by smaller cations [1]. The ideal structure of perovskite is cubic with tolerance factor t (so-called Goldschmidt factor) of 1 ($t = (r_A + r_O)/\sqrt{2(r_B + r_O)}$), where *rA*, *rB* and r*O* are ionic radii of A, B, and oxygen,

respectively) [2]. A t parameter between 0.75 and 1 is necessary to form perovskite structures, with decreasing symmetry for t < 1 [1]. Thanks to the wide range of metals able to adapt in the perovskite structures (about 90 % of metallic elements in the periodic table), the physicochemical properties of perovskite oxides can be finely tuned and they find enormous applications in catalysis for, e. g., steam reforming of toluene [3–5], ethanol [6,7], CH4 [8–10] and bioglycerol [11]; valorization of bio-oil [12–15], biomass [16] and HMF [17], lignin partial oxidation [18,19] and environmental treatments [20–24].

Particulate matter (PM), which is normally referred as soot (although the latter strictly refers only to its carbonaceous fraction), is a noxious emission of diesel engines, which find enormous applications thanks to their high energy efficiency in fuel consumption [25]. PMs can cause a number of respiratory diseases [26] and deactivation of post-treatment's catalysts for the NOx (NO and NO2) reduction processes [27]. Thus, the control of PM's emission is necessary for diesel engine future developments. Generally, there are two steps of PM's treatment: filtration and regeneration [28]. Filtration consists of capturing soot in a Diesel Particulate Filter (DPF), followed by the regeneration which refers to the combustion of soot at relatively high temperature (around 600 °C [29]) to avoid backpressure across the filter [25]. Alternatively, the Continuously Regenerating Trap (CRT) is able to continuously oxidize soot at lower temperature by using NO2 as a stronger oxidant instead of O2 [30,31]. On the other hand, NOx gases, which are also included in diesel exhaust in extremely small quantity, are highly toxic pollutants. NOx elimination is a technical problem because of mandatory requirements to add extra elements to aftertreatment systems, leading to an increase in overall cost of vehicles. A conventional diesel aftertreatment system combines both oxidation catalysts to oxidize trace substances (unburnt hydrocarbon, soot, CO, NO) and a consecutive NOx reduction catalyst. Many efforts have been made to reduce NOx in lean-rich exhaust cycles such as using lean NOx trap (LNT) or NOx storage/reduction (NSR) catalysts. An alternative way is to employ Selective Catalytic Reduction (SCR) by using extra reductants such as NH3 from injected urea solution [32]. These treatments are only productive in case of a large proportion of NO2 present in the exhaust gases [25,33,34]. Therefore, finding catalysts for soot combustion at low temperature while maintaining a high proportion of NO2 for further reduction processes is highly desirable. NOx-assisted soot oxidation is a simultaneous approach which involves NO to NO2 conversion and subsequent soot oxidation by the formed NO2 from the gas phase, at relatively low temperature [28].

Many works have investigated this reaction using noble metal catalysts, which are able to reduce the ignition temperature of soot oxidation (T10% - temperature when 10% of soot is combusted) down to 370 °C, depending on the operating conditions [28,35–38]. However, no high NO2 yields of the soot oxidation reaction have been reported whereas a high proportion of NO2 is beneficial for further NOx elimination processes (for instance, NH3-SCR). Obviously, the applications of noble metals are limited by their prohibitively expensive cost and strategic limitations of availability. Recently, Kim et al. suggested that perovskite La0.9Sr0.1CoO3 can be reasonably priced alternative since it can oxidize about 86% of NO at lower temperature (300 °C) than noble metal rival Pt/Al2O3 [39]. The study has been followed by other works on doped perovskites for low temperature soot oxidation such as LaMn0.9Co0.1O3 [40], BaMn0.7Cu0.3O3 [41], La0.9ACoO3 (A=Na, K and Rb) [23], La1-xBxO3 (B=Ce and Sr) [27] and BaCoO3-λ [42], focusing on the substitution of A- or B-sites to promote redox properties of perovskite oxides by generating either defective structure or multiple oxidation state cations. Furthermore, modified LaCoO3 is generally accepted as a highly active catalyst for NO oxidation [20,43,44], whereas Al2O3 supported oxides are reportedly able to catalyze NOx-assisted soot oxidation at relatively

low temperature [45]. The combination of Al and Co in La-based perovskite oxides may be a promising approach for the NOx-assisted soot oxidation at low temperature. The present work investigates Co-doped LaAlO3 perovskite oxides for soot oxidation in the presence of NOx gases to correlate the catalytic activity with crystallinity, redox properties and the role of lattice oxygen.

2. Experimental section

2.1. Catalyst preparation

LaAl1-xCoxO3 were prepared by the sol–gel method with citric acid. La(NO3)3·6H2O (Sigma-Aldrich,99%), Al(NO3)3·9H2O (Sigma-Aldrich, 99%), Co(NO3)2·6H2O (Sigma-Aldrich,99%) were used as metal precursors and citric acid C6H8O7·H2O as a gel-forming agent. Stoichiometric amounts of nitrate salts were dissolved in deionized water. A suitable amount of citric acid (citric acid:metal =2 mol/mol) was added to the solution where the pH was kept at 7.5 ± 0.5 by dropwise addition of ammonia. The solution was stirred and evaporated at 80 °C until the gel was formed. The gel was then kept at 150 °C for 3 h and at calcination temperature (500, 600 and 700 °C) for 5 h with rampup of 5 °C min^{-1}.

2.2. Catalyst characterization

The BET surface area was determined by N2 adsorption at -196 °C using a Micrometrics Tristar instrument with improved vacuum system. Samples were previously degassed at 250 °C until stable 10 Pa pressure was reached. XRD diffractograms were recorded using Cu Kα (λ=0.15418 nm) radiation in a Bruker D8-Advance device. The reducibility of perovskite oxides was studied by H2-temperature programmed reduction (H2-TPR) using ThermoQuest TPDRO 1100 equipment equipped with TCD detector. The quartz tube reactor was loaded with about 50 mg of sample and pretreated with 10 mL min^{-1} N2 at 500 °C for 30 min and then cooled down to 50 °C. Samples were then heated from room temperature to 950 °C with 5 °C min^{-1} heating rate under 20 mL min^{-1} 5% H2/Ar. O2-Temperature Programmed Desorption (O2-TPD) was conducted in the same instrument. The samples were previously treated under pure O2 flow (40 mL min^{-1}) at 600 °C for 30 min before cooling down to ambient temperature under O2 flow. The desorption was performed from room temperature to 950 °C under He flow (20 mL min^{-1}) with heating rate of 5 °C min^{-1}. The NOx-TPD experiments were conducted in a flow-gas reactor system equipped with ABB Limas and Uras UV and NDIR analyzers to detect NO, NO2, N2O, CO, and CO2 gases separately. Catalysts were placed at the middle position of a 10mm i.d. tubular reactor with thermocouple inserted into the catalytic bed to measure the reaction temperature. In a typical experiment, 200 mg of sample was used. For the NOx desorption tests, NOx (250 ppm NO; 250 ppm NO2, balance N2; total flow 300 mL min^{-1}) was adsorbed at 250 °C until stable concentration of NOx and cooled down to room temperature under N2 flow. The sample was then heated under N2 flow (300 mL min^{-1}) from room temperature to about 600 °C at 5 °C min^{-1}. The XPS experiments were done as reported elsewhere [46]. Briefly, XPS analysis was carried out on an XPS PHI 5000 Versa probe apparatus, using the band-pass energy of 187.85 eV, a 45° take off angle and a 100.0 μm diameter X-ray spot size for survey spectra. High-resolution XP spectra were recorded in the following conditions: pass energy of 23.5 eV, resolution of 0.1 eV, and a step of 0.2 eV. Sample charging effects were eliminated by referring to the spectral line shift of the C 1s binding energy (BE) value at 284.5 eV.

2.3. Activity tests

The NO oxidation tests were conducted in isothermal mode in the same system for NOx-TPD experiments mentioned above. The feed gas contained 650 ppm NO and 5% O2 in N2 (total flow 254 mL min^{-1}) and 200 mg of catalyst was used. The temperature range for the oxidation was 150–400 °C. At each temperature, the stabilization time was about 20–30 min for reaching the steady state reaction in order to avoid the adsorption/desorption effect of NOx on catalysts. NO oxidation was also performed in the temperature ramping mode, in this case the reaction conditions matched those of the NOx-assisted soot oxidation: the feed gas contained 500 ppm NO and 4% O2 in N2 with total flow 600 mL min^{-1} and 200 mg of catalyst with ramping rate 5 °C min^{-1}. Besides the LaAl1-xCoxO3 catalysts Pt/Al2O3 with 5% Pt loading (Sigma-Aldrich 205974) was used as commercial reference.

The activity of the catalysts in NOx-assisted soot oxidation tests was determined by Temperature Programmed Reaction (TPR) with heating rate of 5 °C min^{-1}. The soot oxidation was studied by mixing 20 mg of soot (Printex U, a carbon black used as model soot) with 180 mg of catalyst or SiC for the reference non-catalytic test (catalyst:soot=9:1) in loose contact. Feed gas contained 500 ppm of NO and 4% oxygen in a flow of N2 as balance gas, the total flow being 600 mL min^{-1}. The tests were conducted between 200 °C and 700 °C with a ramp of 5 °C min−1. The soot conversion and CO2 selectivity were calculated as followed:

$$\text{Soot conversion (\%)} = \frac{\sum_0^t (co_2+co)}{(co_2+co)_{total}} 100 \qquad \text{CO}_2\text{ selectivity (\%)} = \frac{\sum_0^t (co_2)}{(co_2+co)_{total}} 100$$

3. Results and discussion

3.1. Characterization

3.1.1. Structural properties

X-ray diffraction patterns of all catalysts LaAl1-xCoxO3 (x=0, 0.25, 0.5, 0.75 and 1) calcined at 700 °C are shown in Fig. 1. All catalysts exhibit a well-crystallized perovskite phase, which is the only phase present from x=0 to 0.5 and is accompanied in LaAl0.25Co0.75O3 and LaCoO3 by two minor peaks at 2θ of about 36.7 and 28.1°, which belong respectively to Co3O4 and La2O3. The perovskite phase presents symmetric diffraction peaks in the case of LaAlO3, whereas peak splitting is observed with increasing cobalt. Rietveld analysis has been conducted on all catalysts calcined at 700 °C to understand the lowering of symmetry with Co-doping. The refinement was done with the Thompson-Cox-Hastings pseudo-Voigt peak profile and two space groups: rhombohedral R-3c and cubic Pm-3 m. The refinement data, reported in Table 1, confirm the change of perovskite symmetry with the composition, LaAlO3 being cubic and all other samples being rhombohedral. Interestingly, all samples would be expected presenting R-3c space group at room temperature [47]. Rhombohedral perovskite normally evolves towards cubic structure when the octahedral tilting is reduced at higher temperature. LaAlO3 is normally rhombohedral at room temperature, reaching space group Pm-3m at nearly 530 °C [47,48]. The presence of cubic phase at room temperature is probably due to a metastability effect. Substituted LaAl perovskites remain rhombohedral also at very high temperature and, in the case of LaCoO3, the rhombohedral structure is also stable above 970 °C [48,49]. In the case of solid solutions intermediate between LaAlO3 and LaCoO3, Aswin et al. observed that the rhombohedral phase was accompanied by a

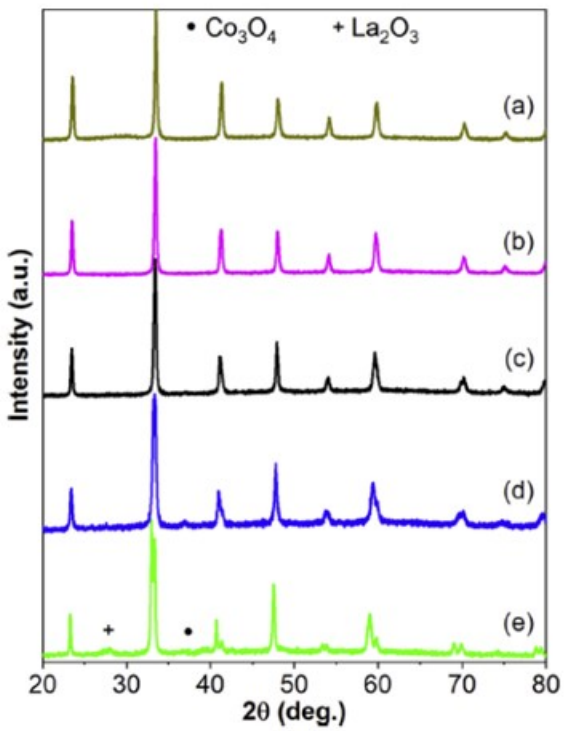

Fig. 1. X-Ray diffractions of LaAl1-xCoxO3 calcined at 700 °C: (a) x=0; (b) x=0.5; (c) x=0.5; (d) x=0.75; (e) x=1.

secondary monoclinic perovskite phase [50]. No monoclinic phase was observed in our samples. It is tempting to assume that the presence of such a phase is a secondary result of sintering at 1030 °C in the preparation of Aswin et al.

The volume of the formula units LaAl1-xCoxO3 calculated from the cell parameters, taking into account Z=1 for Pm-3m and Z=6 for R-3c space groups, are reported in Table 1 and highlighted in Fig. 2a. They show a systematic increase of volume from LaAlO3 to LaCoO3 once the R-3c symmetry is established, indicating that Co is well incorporated inside the perovskite framework. In fact, trivalent Co is larger than Al3+ [51], so the substitution of Al by Co tends to expand the unit cell.

Table 1.

Refinement parameters of LaAl1-xCoxO3 calcined at 700 °C.

$LaAl_{1-x}Co_xO_3$ (x)	Space group	a (Å)	c (Å)	Formula unit volume ($Å^3$)
0	**Pm-3m**	3.7927(1)	–	54.556(2)
0.25	**R-3c**	5.3673(2)	13.117(1)	54.542(3)
0.5	**R-3c**	5.3772(2)	13.101(1)	54.882(1)
0.75	**R-3c**	5.4046(2)	13.108(1)	55.263(3)
1	**R-3c**	5.4427(2)	13.126(1)	56.122(3)

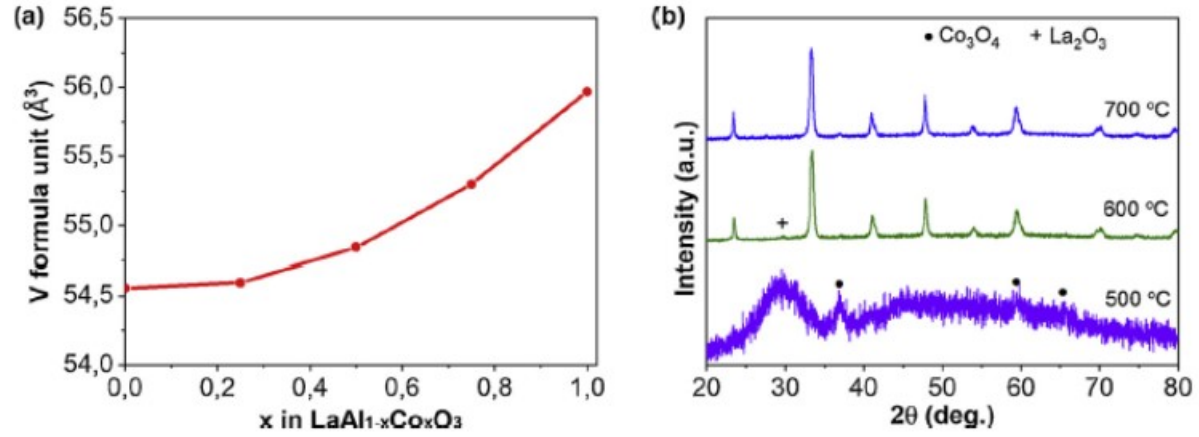

Fig. 2. (a) Volume of the formula units LaAl1-xCoxO3 as a function of the cobalt fraction; (b) diffraction patterns of LaAl0. 25Co0.75O3 calcined at different temperatures.

The effect of calcination temperature on the formation of the perovskite phase is highlighted in Fig.2b, in which the diffraction patterns of LaAl0.25Co0.75O3 calcined at 500, 600 and 700 °C are shown. The diffraction pattern at 500 °C present no perovskite peaks but exhibits broad bands of Co3O4 and La2O3 phases. Evaluation of the peaks of these phases by the Scherrer method suggests sizes of 27 nm for Co3O4 and 2.6 nm for La2O3, a signature of nano-crystalline form for this last phase. At 600 °C, the perovskite structure emerges beside traces of La2O3 phase, better crystallized than at 500 °C. La2O3 disappears altogether at a calcination temperature of 700 °C, leaving perovskite as the only crystalline phase.

The textural properties of LaAl1-xCoxO3 calcined at 700 °C are listed in Table 2. The average crystallite size of LaAl1-xCoxO3 is calculated from the Rietveld refinement by the Williamson-Hall method. Crystallite size dc slightly varies around 30 nm for x=0 to 0.75, before jumping up for the total introduction of cobalt. The surface areas of all samples, measured by N2 sorption, are between 10–15 m2 g^{-1}, as expected for samples annealed at high temperature [52]. It can be observed that the observed variation in crystallite size does not correspond to any equivalent change in surface area. Indeed, taking into account the density of the perovskite, the observed surface areas correspond to grain size between 60 and 80 nm, in good agreement only with the crystallite size of LaCoO3. It is tempting to advance the hypothesis that, in the case of all other samples, the 30 nm crystallites are the result of splitting of larger grains during the thermal treatment.

$LaAl_{1-x}Co_xO_3(x)$	d_c (nm)	S_{BET} ($m^2\ g^{-1}$)	V_p ($cm^3 g^{-1}$)
0	30.5	14.4	0.10
0.25	32.1	11.4	0.09
0.50	36.8	11.6	0.09
0.75	28.7	13.1	0.08
1.0	73.7	12.3	0.08

Table 2. Textural properties of LaAl1-xCoxO3 calcined at 700 °C.

3.1.2. Redox properties

Fig. 3 summarizes the H2-TPR profiles of LaAl1-xCoxO3 (x=0, 0.25, 0.5, 0.75, 1) calcined at 700 °C and LaAl0.25Co0.75O3 calcined at 500, 600 and 700 °C. In the literature, the reduction of Co^{3+} in LaCoO3 was generally proposed by two different pathways, implying one or two steps. In the two-steps route, $Co3^{+}$ is converted to Co0 via Co^{2+} in two distinguished temperature regions at around 420 °C for Co^{3+} to Co^{2+} and 550 °C for $Co2^{+}$ to Co^{0} with the formation of intermediate brownmillerite LaCoO2.5 [16,53–57]. This two-steps mechanism should be confirmed by the area ratio of the first peak to the second one of 1:2 [58]. However, the H2 consumption in the high-temperature reduction region is usually found lower than expected [44,55,59], suggesting that Co^{0} might be partially formed in the first stage at lower temperature [55,60]. Indeed, the Co^{3+} reduction was also proposed as one-step mechanism, in which Co0 can be produced directly from Co^{3+} with the formation of oxygen-deficient compound LaCoO3-y, bypassing the Co^{2+} species [60], and splitting of the reduction peak can be attributed to different structural Co3+ species related to the distortion of perovskite structure and oxygen defects [61].

The TPR profile of the as-prepared LaCoO3 reveals two separate peaks with maxima at ca. 395 and 580 °C (Fig. 3a). The H2-consumption, reported in Table 3, corresponds to a 1.5 H2/Co ratio, indicating that all Co3+ has been reduced to Co0. The H2-consumption ratio between the first and second reduction peaks is 1.04/1, indicating that the first peak does not correspond only to the reduction of Co^{3+} to Co^{2+} but includes some further reduction of Co^{2+}. The mechanism of reduction

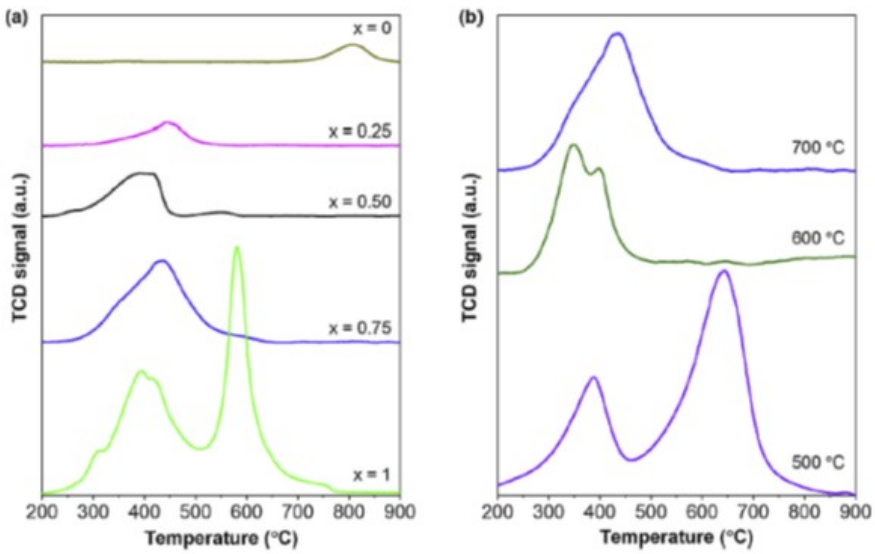

Fig. 3.

H2-TPR profiles of the samples LaAl1-xCoxO3 calcined at 700 °C (a); LaAl0.25Co0.75O3 calcined at different temperatures (b).

Catalysts	X	Peak temperature (°C)	H_2-consumption (μmol g^{-1})	H_2/Co mol/mol
$LaAlO_3$	0.00	–	–	–
$LaAl_{0.75}Co_{0.25}O_3$	0.25	445	1202	1.07
$LaAl_{0.50}Co_{0.50}O_3$	0.50	394	2909	1.34
$LaAl_{0.25}Co_{0.75}O_3$	0.75	437	4909	1.56
$LaCoO_3$	1.00	395, 580	6379	1.57

Table 3.

H2-consumption of LaAl1-xCoxO3 with different composition.

seems hence to be a mixed one-step and two-steps process. The first reduction peak presents several components: the small shoulder located at 310 °C can be ascribed to microcrystalline part or chemisorbed oxygen in the catalyst surface [20]. The two overlapping components at 391 and 418 °C probably include the formation of Co^0 at relatively low temperature [55,60].

When Al partially replaces Co in LaCoO3, the H2-TPR profiles of LaAl1-xCoxO3 follow the one–step reduction mechanism from around 210 °C to 600 °C. The H2/Co ratio (Table 3) is close to the values of total reduction for LaAl0.25Co0.75O3, indicating that Co^{3+} is completely reduced to Co^0 up to around 600 °C. This suggests that, in bimetallic Al-Co perovskites, Co^{3+} can be reduced to metallic species at low temperature without any clear intermediate formation of Co^{2+}, and the asymmetry of peak shape may be due to variously distinct Co^{3+} species in perovskite lattice [61]. LaAl0.5Co0.5O3 and LaAl0.75Co0.25O3, the most Al-rich mixed samples, present a H2-consumption lower than the value expected for complete reduction of Co^{3+} (Table 3). This effect could be attributed to a lower than expected average oxidation state of cobalt, probably related to cation vacancies. In the case of the Co-free LaAlO3, a small peak observed above 800 °C is not related to reduction phenomena but corresponds to CO2 release from decomposition of carbonate species from the surface of this highly basic solid.

Fig. 3b shows H2-TPR profiles of LaAl0.25Co0.75O3 calcined at 500, 600 and 700 °C. The sample annealed at 500 °C exhibits two peaks at 388 and 646 °C. The first peak closely correspond to the expected temperature for reduction of the Co3O4 phase observed in the sample [62]. The second peak does not correspond to a reduction peak but it is at the temperature expected for the decarbonation of the carbonate species at the surface of the extremely dispersed La2O3 evidenced by the XRD pattern [63]. LaAl0.25Co0.75O3 calcined at 600 °C reveals two overlapped peaks at

350 and 398 °C. This corresponds to the formation of Co0 by reduction of perovskite LaAl0.25Co0.75O3 at a temperature nearly 90 °C lower than in the case of the same material calcined at 700 °C. This may be linked with lower surface area, narrower crystal size distribution and higher crystal size with higher calcination temperature, which leads to more diffusional resistance [24].

It is generally accepted that perovskite LaCoO3 exhibits two type of desorbed oxygen. The α-oxygen, which is desorbed below 750 °C, is usually ascribed to oxygen weakly bound to perovskite surface. β-oxygen is lattice oxygen which diffuses from bulk and it is considered as an indicator of oxygen mobility in the structure [54,59,64,65]. The latter species can come from inner bulk oxygen vacancies or can be directly associated with the B-site cation reduction in the perovskite oxide framework [56]. LaCoO3 shows two desorption peaks at around 650 °C and 827 °C, probably corresponding to α- and β-oxygen, respectively (Fig. 4). LaCoO3 releases 77.5 μmol g^{-1} of β-oxygen (nearly 2% of bulk oxygen), as a result of Co^{3+} to Co^{2+} reduction and anion vacancy generation [20,64]. The amount of β-oxygen release from LaCoO3 and the desorption temperature are comparable with the results of other groups [66,67]. Decreasing the cobalt fraction x from 1 to 0.75 significantly raises the quantity of β-oxygen, LaAl0.25Co0.75O3 releasing 158.1 μmol g^{-1} at a lower desorption temperature of 849 °C. The oxygen species in LaAl0.25Co0.75O3 occupies almost 3.7% of total oxygen anion in perovskite, revealing the highest oxygen mobility among the studied samples.

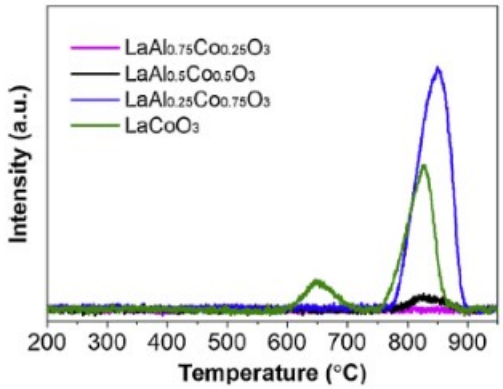

Fig. 4. O2-TPD profiles of LaCo1-xAlxO3 samples calcined at 700 °C.

It should be noticed that Royer et al. suggested that β-oxygen is likely to originate from grain boundaries between two neighbor crystal domains due to higher oxygen diffusivity within boundaries than bulk, and the feature was significantly enhanced by substituting 20% of Co by Fe to form LaCo0.8Fe0.2O3 [66]. Therefore, the highest amount of lattice oxygen for LaAl0.25Co0.75O3 may be related to the smallest crystallite size among the studied samples. For further decrease of cobalt content, the oxygen evolution dramatically drops to 9.1 μmol g^{-1} when 50% of Co is replaced by Al and no β-oxygen is measured when only 25% cobalt is left (Table 4). LaAl0.75Co0.25O3 exhibits no oxygen evolution during the experiment, as it is the case for LaAlO3 due to non-reducibility of aluminum cations. The decrease of β-oxygen with the increase of cobalt content closely matches the decrease of H2-consumption in H2-TPR and confirms that the cobalt-richest samples present abundant cation vacancies and a lower than expected cobalt oxidation state.

Samples	β-O_2-desorption (μmol g^{-1})	O-percentage (mol.%)	Temperature (°C)
$LaAl_{0.75}Co_{0.25}O_3$	–	–	–
$LaAl_{0.50}Co_{0.50}O_3$	9.1	0.2	827
$LaAl_{0.25}Co_{0.75}O_3$	158.1	3.7	849
$LaCoO_3$	77.5	1.9	827

Table 4. Calculated quantity of desorbed oxygen of LaAl1-xCoxO3 obtained by integration of O2-TPD profiles.

3.1.3. Surface properties

The Fig. 5a shows XPS profiles of LaAl1-xCoxO3 (x=0, 0.25, 0.5 and 0.75) with Co 2p3/2 and 2p1/2 binding energy at 780–780.4 eV and 795.4 eV respectively, both ascribed to Co3+ species [67,68]. Moreover, distorted 2p3/2 Co pattern is distinctive for Co^{3+} species [69], with a similar gap between 2p1/2–2p3/2 of 15.4 eV [70] and no Co^{2+} shake up peaks at 785–788 eV [69] [71], suggesting that mainly Co^{3+} species can be detected at the surface of the prepared samples. However, the satellite signal at 790.2 eV and broadening region at about 805 eV can be seen in LaAl0.5Co0.5O3, and more pronounced in the sample with more cobalt: LaAl0.25Co0.75O3. This

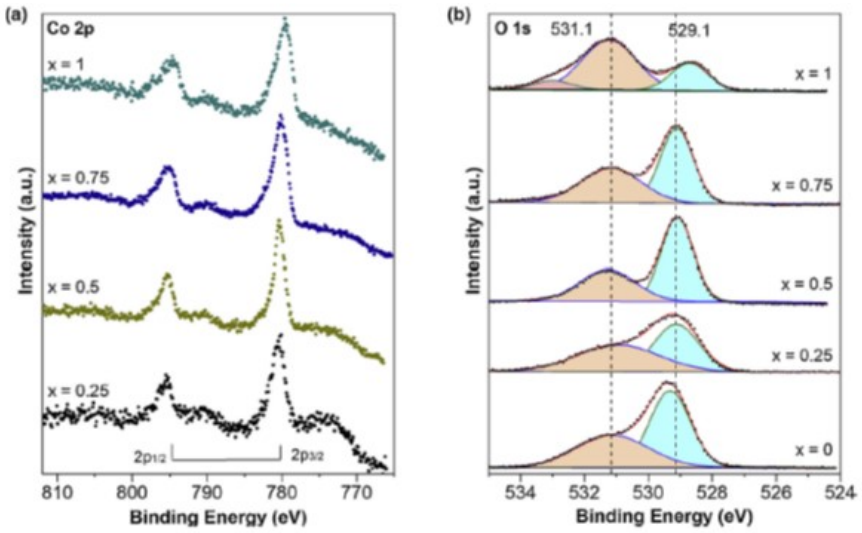

Fig. 5. XPS spectra of Co 2p (a) and O 1s (b) of LaAl1-xCoxO3 (x=0, 0.25, 0.5, 0.75, 1).

Table 5. Relative abundances of oxygen species derived from the deconvolution of O 1s XPS spectra and Co/Al surface ratio.

Sample	$(Co/Al)_{surf.}$	Co $2p_{3/2}$	O_{ads}		O_{lat}		O_{ads}/O_{lat}
		BE (eV)	BE (eV)	%-atom	BE (eV)	%-atom	
$LaAlO_3$	0	–	531.1	43.5	529.3	56.5	0.77
$LaAl_{0.75}Co_{0.25}O_3$	0.4	780.4	531.2	44.4	529.2	55.6	0.80
$LaAl_{0.5}Co_{0.5}O_3$	0.6	780.4	531.3	39.4	529.1	60.6	0.65
$LaAl_{0.25}Co_{0.75}O_3$	3.2	780.0	531.1	42.9	529.1	57.1	0.75
$LaCoO_3$	–	779.5	531.2	66.2	528.7	25.4	2.60

profile is reported for Co3O4 [72], indicating that there may be some cobalt oxides not incorporated in perovskite structure when more than 50% of Al is replaced by Co, which is in agreement with XRD profiles. Table 5 listed the ratios of surface Co/Al which increase from 0.4 for LaAl0.75Co0.25O3 to 3.2 for LaAl0.25Co0.75O3. This ratio for LaAl0.75Co0.25O3 is higher than its bulk composition (0.33) by around 20% and the surface is slightly enriched with Co. By contrast, LaAl0.5Co0.5O3 has surface Co lower than in the bulk composition: 0.6 in comparison with theoretical 1.0.

The O 1s XPS spectra are deconvoluted to two oxygen species: peaks at 529.1–529.3 eV are characteristic of surface lattice oxygen (denoted as Olat) and signals at 531.1–531.3 eV can be ascribed to oxygen adsorbed on perovskite surface (denoted as Oads) [73,74] (Fig. 5b). Concerning the LaCoO3 sample, its O 1s curve was satisfactorily curve-fitted by using 3 peaks. Besides the two components previously described, the signal at higher BE (533 eV) has been assigned to O species in some segregated oxide phases. Such an assignment is in agreement with the XRD pattern

of the sample, in which the main peak of the La2O3 and Co3O4 phases was detected (see Fig. 1). The ratios Oads/Olat of LaAl1-xCoxO3 with x=0, 0.25, 0.5 and 0.75 are 0.77, 0.80, 0.65 and 0.75, respectively (Table 5). These four samples, with similar surface area, show Oads/Olat ratios in the same range, whereas the LaCoO3 sample, with much lower surface area, shows a much higher Oads/Olat surface ratio. These data clearly indicate that the oxygen distribution at the surface in non-reactive conditions poorly reflects the bulk mobility of oxygen as revealed by H2-TPR or O2-desorption experiments. The quantity of Oads is relatively correlated to surface area values which are similar for LaAlO3.

3.1.4. NOx-temperature programmed desorption

For the NOx-TPD measurement, the samples were adsorbed by equal quantities of NO and NO2 (about 250 ppm of each balanced by N2) at 250 °C until the saturation, cooled down under N2, and followed by heating up under N2 atmosphere with a rate of 5 °C min^{-1}. Fig. 6a reveals the NOx-TPD profiles of LaAl1-xCoxO3 (x up to 0.75), while a similar figure for LaCoO3 is plotted in Fig. 6c. The first small NOx desorption can be ascribed to physically adsorbed species which peaks at about 150 °C for LaAlO3, and decreases by around 60 °C when Al is substituted by Co. It is reported that the NOx desorption below 250 °C is mostly related to B-site of perovskite, while at high temperature the basic A-site may take a role [44]. The adsorbed species is reportedly in dependence with adsorption temperature [75]. When NOx is adsorbed below 250 °C, it is mainly stored as nitrite species, which can convert Fig. 4. O2-TPD profiles of LaCo1-xAlxO3 samples calcined at 700 °C. into nitrate at higher adsorption temperature [75]. In contrast, at high temperatures NOx can be released by the nitrate decomposition followed by the oxides formation and the destruction of perovskite structure. [42]. It is also suggested that at low adsorption temperature NOx is stored as chemisorbed NOx and converted to nitrate by interaction with surface hydroxyl groups [76]. This chemisorbed species may be unstable, and it can be released during TPD experiment up to 350 °C.

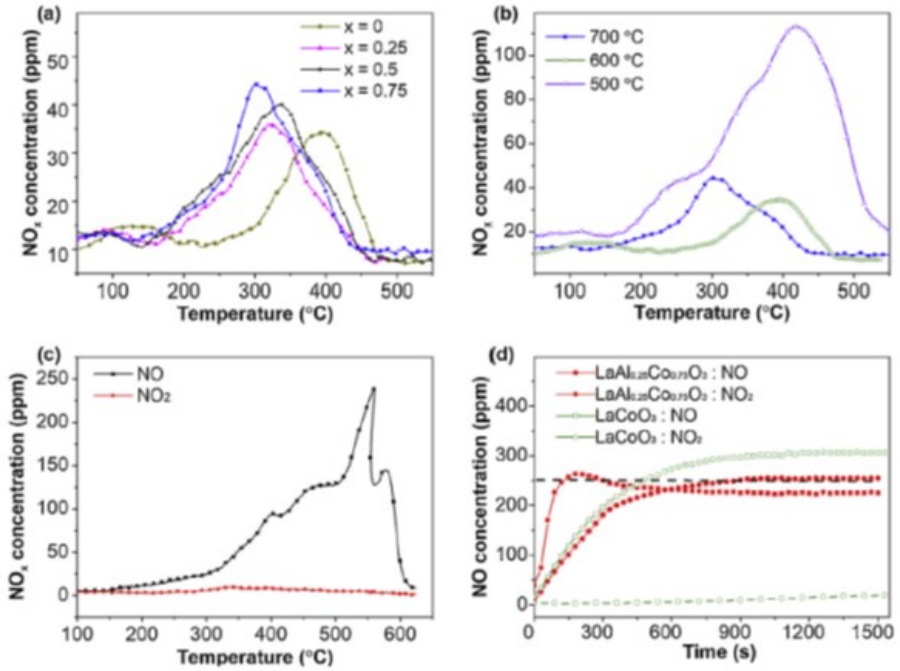

Fig. 6.

NOx desorption curves of (a) LaCo1-xAlxO3 calcined at 700 °C and (b) LaAl0.25Co0.75O3 calcined at different temperatures; (c) NOx desorption of LaCoO3 at 250 °C with time (250 ppm of NOx and 250 ppm of NO2 balance in N2; 250 °C); (d) NOx adsorption on LaCoO3 and LaAl0.25Co0.75O3 at 250 °C.

Generally, NO2 is desorbed at a lower temperature in all studied samples compared to NO [77], and its desorption temperature drops with increased Co doping, from 351 °C for LaAlO3 to 275 °C for LaAl0.25Co0.75O3, and almost disappears in case of LaCoO3 (Table 6). The quantity of desorbed gases is similar in all cases except LaCoO3, varying from around 53 to 75 μmol g^{-1}. The values partially depend on the surface area which may be not promoted by high calcination temperature of perovskite oxides. Furthermore, deficient perovskites favor NO adsorption on oxygen vacancies before oxidizing to NO2 [43,78] which may not be found in our compounds persevering charge neutrality.

Catalysts	NO_2		NO		Total (μmol g^{-1})
	Amount (μmol g^{-1})	T_{max} (°C)	Amount (μmol g^{-1})	T_{max} (°C)	
$LaAlO_3$	26.8	351	26.2	412	53.0
$LaAl_{0.75}Co_{0.25}O_3$	27.8	294	25.8	347	52.9
$LaAl_{0.5}Co_{0.5}O_3$	36.5	289	38.7	350	75.2
$LaAl_{0.25}Co_{0.75}O_3$	24.7	275	36.3	320	61.0
$LaCoO_3$	–	–	410.2	558	411.7

Table 6. Desorbed NOx quantity and relative desorption temperature of LaAl1-xCoxO3.

NO desorption temperature has the same trend of NO2 but at a higher temperature. It decreases with Co content from 412 °C for LaAlO3 to a similar range of 347–350 °C for both LaAl0.75Co0.25O3 and LaAl0.5Co0.5O3, and drops to the minimum of 320 °C for LaAl0.25Co0.75O3. Surprisingly, a decrease in Al quantity weakens the bond with acidic NOx, leading to lower desorption temperature. The introduction of Co may induce some modifications of the perovskite surface which leads to variation in desorption temperature of NOx [44]. It is reported that calcination temperature up to 1000 °C induces the formation of oxygen-deficient BaCoO3-λ which promotes the trap of NOx on oxygen vacancies; however, when the synthesis temperature is lower than 700 °C, surface areas may significantly contribute to the quantity of absorbed species [42]. For the sample LaAl0.25Co0.75O3 calcined at different temperatures (Fig. 6b), the one annealed at 500 °C releases the most NOx with a value of 258 μmol g^{-1} in comparison with 45 and 61 μmol g^{-1} of LaAl0.25Co0.75O3 calcined at 600 and 700 °C respectively. On the other hand, the specific surface areas of the sample decrease from ~22 to ~16 m2 g^{-1} with calcination temperature from 500 to 600 °C, and drops to 13.1 m^2 g^{-1} at 700 °C. Furthermore, it can be seen that calcination temperature from 700 to 600 °C shifts the desorption peak of NOx by around 96 °C, whereas sample calcined at 500 °C possesses the highest desorption temperature at 420 °C. The presence of La2O3 in the samples calcined at low temperatures may be attributed to a stronger bond with NOx and higher adsorbed quantity since La2O3 is supposed as the main NOx storage site [43].

In many works for NOx storage and reduction, NO is fed with O2 to be oxidized to NO2 which is more readily trapped by basic catalysts [77]. In the present study, NO and NO2 are supplied in an approximately equal amount at 250 °C without the presence of O2. However, NO2 almost disappears while NO is higher than its original value (250 ppm) during the adsorption process over LaCoO3 (Fig.6d). This behavior cannot be found in other samples (for example LaAl0.25Co0.75O3 in Fig. 6d) where both NO and NO2 gets saturated after around 10 min. This suggests that during the NOx adsorption at 250 °C, NO2 may be adsorbed and partially reduced to NO. This is confirmed by the presence of more intense peaks of Co3O4 and La2O3 phases in XRD pattern of LaCoO3 after TPD treatment, which may be a result of Co^{3+} to Co^{4+} oxidation by NO2 reduction. Moreover, the NOx-TPD of LaCoO3 shows no NO2 peaks whereas NO is

desorbed at significantly higher than those of other samples (Fig. 6c). The difference between NO adsorption (calculated by integration of NO adsorption curve with time) and desorption is 88.2 μmol g^{-1}, indicating the additional amount of NO from NO2 reduction. It should be mentioned that NO2 can be adsorbed by basic La2O3 observed in XRD pattern for LaCoO3 to form nitrate salt, which can be decomposed at higher temperature than that in the experiment [79]. It may be suggested that NO2 may be adsorbed on LaCoO3 and completely reduced to other species together with both Co^{4+} formation and partially perovskite structure collapse.

3.2. Catalytic activities

3.2.1. NO oxidation

The NO oxidation tests aim at investigating the NO2 production at low temperatures, which is beneficial for the NOx storage/reduction process and soot combustion [77]. Fig. 7a shows NO to NO2 conversion profiles obtained from the isothermal mode, whereas the dashed line represents the thermodynamic equilibrium of NO oxidation reaction as a reference. The peaks of the curves indicate the temperatures where maximum NO2 generation is achieved. At temperatures below the peak temperature the NO oxidation is kinetically limited, while at higher temperatures the thermodynamic equilibrium is the limiting factor. Among the as-prepared samples, LaAl0.25Co0.75O3 perovskite presents the best performance (Table 7), with a maximum NO conversion of about 78% at 320 °C.

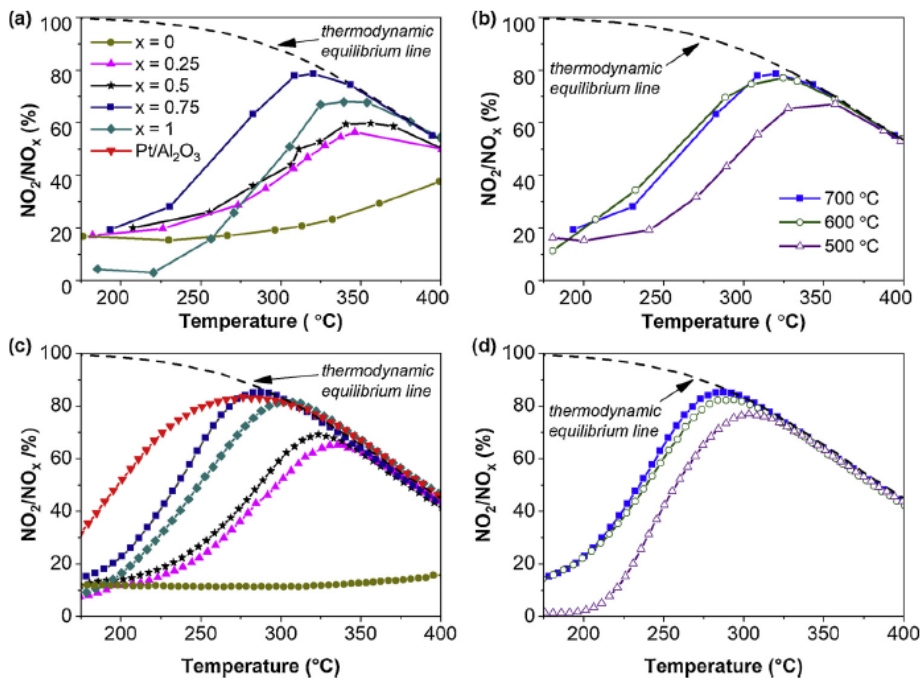

Fig. 7. NO2 percentage of (a) LaAl1-xCoxO3 calcined at 700 °C and (b) LaAl0.25Co0.75O3 calcined at different temperatures in steady state conditions and (c) LaAl1-xCoxO3 calcined at 700 °C and (d) LaAl0.25Co0.75O3 calcined at different temperatures in dynamic conditions.

Catalysts	$LaAl_{1-x}Co_xO_3$ (x)	NO_2/NO_x (%)	Temperature (°C)
$LaAlO_3$	0	38	399
$LaAl_{0.75}Co_{0.25}O_3$	0.25	56	346
$LaAl_{0.5}Co_{0.5}O_3$	0.5	60	356
$LaAl_{0.25}Co_{0.75}O_3$	0.75	78	320
$LaCoO_3$	1	68	339

Table 7. NOx performances of LaCo1-xAlxO3 calcined at 700 °C.

In contrast, LaAlO3 exhibits the worst activity with 38% at a remarkably high temperature of about 399 °C and the NO conversion increases with Co, from 38% for LaAlO3 to 56 and 60% for LaAl0.75Co0.25O3 and LaAl0.5Co0.5O3 catalysts, respectively. The conversion reaches the maximum value for LaAl0.25Co0.75O3 before reverting to 68% when Al is totally substituted by Co as reported for LaCoO3 [20]. The same catalysts were also tested in the temperature ramping mode and under lower residence time (Fig. 7c and d) in order to obtain the same test conditions as the soot oxidation tests and to get a closer correlation between the two kind of experiments. As can be appreciated, the order of the catalytic performance (LaAl0.25Co0.75O3 > LaCoO3 > LaAl0.5Co0.5O3 > LaAl0.75Co0.25O3 > LaAlO3) was the same in both steady state and dynamic conditions.

Furthermore, by comparing the LaAl0.25Co0.75O3 sample with a Pt/Al2O3 commercial oxidation catalyst, the NO oxidation rate of the perovskite is obviously lower although the equilibrium is reached by both catalysts at almost the same temperature, which is the one of interest for the soot oxidation, offering a viable alternative for the PGM-based catalysts under certain conditions. It should be noticed that NO-to-NO2 oxidation ability is due to the generation of oxygen defects and redox property [80], which can be created by adjusting cation doping at A or B sites in the perovskite compounds. Others suggest that higher oxidation capacity is associated with higher oxygen mobility and exchange between lattice oxygen and gas phase oxygen [20]. This may be related to LaAl0.25Co0.75O3 with the higher amount of β-oxygen desorption (Table 4), implying the pivotal role of lattice oxygen species in the improvement of the oxidation reaction.

Furthermore, all samples have negligible α-oxygen quantity released during O2-TPD experiment, but still possess comparable NO oxidation activity. This result indicates that surface oxygen may not play a critical role in NO oxidation but the diffusion of lattice oxygen to the surface is more important [81]. However, LaCoO3 desorbs significantly more oxygen than its rivals (LaAl0.75Co0.25O3 and LaAl0.5Co0.5O3) but its oxidation activity worsens despite more Co content. The higher NOx desorption temperature for LaCoO3 indicates strong interactions between NOx and the catalyst, while partial doping Al slightly weakens the bonds facilitating the NOx release at low temperatures. Thus, oxygen mobility may be not the only factor for NO oxidation but the synergetic interaction between two B-site cations (Al and Co) may enhance oxidation performance of the catalysts, as suggested by Ma et al. with a small substitution of Co by Fe to promote NO conversion [82]. Furthermore, under H2/Ar flow in the H2-TPR experiment, LaAl0.25Co0.75O3 is reduced at a temperature of 437 °C, higher than 394 °C for LaAl0.75Co0.25O3. However, the NO conversions of these samples reveal different trend for the reduction temperature, which may imply the negligible effects of reducibility on NO oxidation. Furthermore, LaCoO3 produces less NO2 at low temperatures but higher above 275 °C than LaAl0.75Co0.25O3 and LaAl0.5Co0.5O3 (Fig. 7a). This may be related to the fact that LaCoO3 can adsorb NO2 at low temperatures and partially reduce to NO, as can be seen in the NOx-TPD experiment. Besides, the temperature of maximum NO2 production is lowest for LaAl0.25Co0.75O3 at 320 °C, and increases by around 30 °C with x=0.25 and 0.5 (Table 7). A similar trend can be found for NO desorption profiles (Table 6), where NO desorbs at 320 °C for LaAl0.25Co0.75O3 and increase to 350 and 347 °C for LaAl0.5Co0.5O3 and LaAl0.75Co0.25O3 respectively. This highlights the suggestion in which the oxidation reaction commences with the chemisorption of reactants NO and O2, followed by the dissociation of O2 and NO2 on the surface [28].

Many works have found that substitutions of A-site generate oxygen vacancies, for example La1-xSrxBO3 [20,43], or of B-site to support the co-existence of multivalent states, e.g. LaCo1-

xMgxO3 [67], in order to promote NO oxidation. Furthermore, it was shown that the partial substitution of cations can promote the formation of preferential oxidation active states (e.g. metallic isolated or biactive sites) that can promote the NO oxidation [83,84]. However, there are fewer investigations regarding the effect of the degree of perovskite crystallinity on the NO oxidation. Fig. 7b shows profiles of NO2 molar percentage in the NOx mixture of LaAl0.25Co0.75O3 which is calcined at 500, 600 and 700 °C. It is clear that the sample annealed at 500 °C reveals the lowest oxidation activity, with about 66% at ˜ 350 °C despite the highest surface area (21.9m2 g−1), probably due to the presence of segregated phases such as Co3O4 and La2O3 [20]. The samples calcined at 600 °C show superior oxidation performances at low temperatures, but at above 300 °C the solid calcined at 700 °C slightly outperforms. Despite the reduction in surface area, the calcination temperature up to 700 °C has positive effects on oxidation activity, which may be associated with higher crystallinity and less minor phases as detected in XRD profiles (Fig. 2b). However, further increase calcination temperature beyond 700 °C may lead to deterioration of oxidation activity due to low surface area as studied elsewhere [20].

3.2.2. Soot oxidation

Fig. 8 reveals the results of soot oxidation tests over LaAl0.25Co0.75O3 (calcined at 700 °C) in the presence and absence of NOx gas. Table 8 shows the testing outputs: T10% represents the ignition temperature, when 10% of soot is burnt; T50% and T90% are the temperatures when 50% and 90% of soot is consumed respectively; Tmax is the temperature when maximum CO2 production is achieved, and (NO2/NOx)max/T is the maximum percentage of NO2 over NOx mixture and its temperature. Generally, the NOx-assisted soot oxidation reaction starts with the oxidation of adsorbed NO to produce NO2, which is a stronger oxidant than O2 [38,45,85]. Soot can be also oxidized by O2 but at a relatively higher temperature than with NO2. In the presence of NO2, it interacts with soot surface to form surface oxygen complexes (SOC), which decomposes further to CO, CO2 and NO [28,86]. O2 is first adsorbed at the catalyst's surface and undergoes the dissociation to form active oxygen species. This species is possibly transferred to the surface of soot forming SOC via spill-over mechanism [86]. The results clearly show that soot is oxidized at a significantly lower temperature in the presence of NOx (T10% are 377 and 513 °C for with and without NOx respectively).

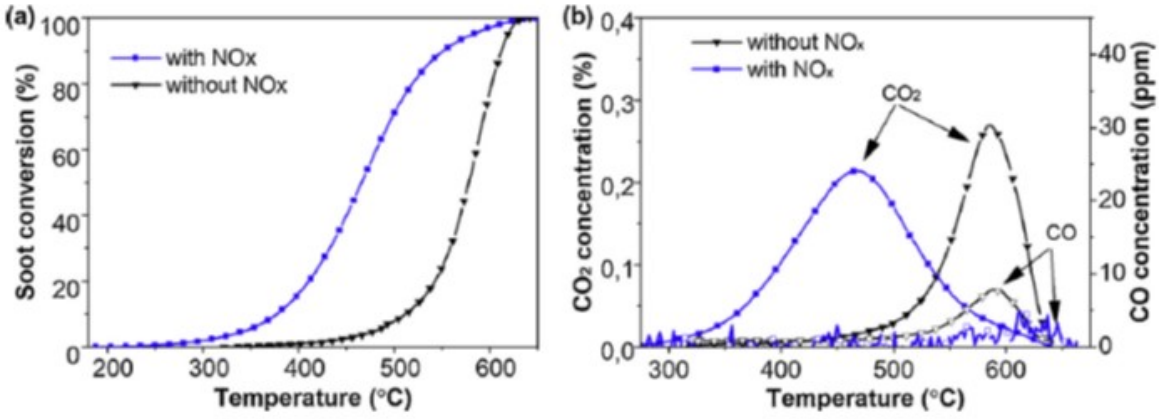

Fig. 8. (a) Soot conversion and (b) CO2 and CO concentration as function of temperature during soot oxidation catalytic tests with and without NOx supply over LaAl0.25Co0.75O3 catalyst.

Table 8. Catalytic performances of LaCo1-xAlxO3 calcined at 700 °C.

$LaAl_{1-x}Co_xO_3$	x	$T_{10\%}$ (°C)	$T_{50\%}$ (°C)	T_{max} (°C)	$T_{90\%}$ (°C)	$(NO_2/NO_x)_{max}$/T(°C)	CO_2 selectivity (%)
$LaAlO_3$	0	470	562	563	623	0.08/376	82.3
$LaAl_{0.75}Co_{0.25}O_3$	0.25	402	484	481	560	0.39/383	98.7
$LaAl_{0.5}Co_{0.5}O_3$	0.5	401	487	482	570	0.44/379	98.1
$LaAl_{0.25}Co_{0.75}O_3$	0.75	377	467	467	585	0.71/321	99.8
$LaCoO_3$	1	389	467	493	624	0.40/352	93.8
Without NO_x	–	513	578	587	612	-/-	98.5
SiC	–	532	610	626	640	-/-	50.7

Moreover, NOx also remarkably supports to reduce the temperature of 50% of soot conversion by around 111 °C although at higher temperatures the role of NOx in soot oxidation becomes less prominent with the decrease of T90% by only 27 °C because of limited NOx availability (Table 8). In terms of CO2 production, NOx promotes the total oxidation with CO2 selectivity of 99.8% compared to 98.5% of that without NOx. Without the presence of NOx, the Tmax increases by around 120 °C and the formation of CO is significant. The results highlight the vital role of NO2 in soot oxidation and its further applications in NOx reduction process by the selective catalytic reduction reaction.

Fig. 9 summarizes soot conversion, NO2/NOx percentage, CO and CO2 concentrations as functions of temperature during the experiments with NOx-assisted soot oxidation over LaAl1-xCoxO3 catalysts. Among the prepared solids, LaAlO3 possesses certainly the lowest activity with T10%, T50% and T90% of 470, 562 and 623 °C respectively. Doping Co shifts the reaction temperature to lower ranges, LaAl0.75Co0.25O3 obviously outperforms LaAlO3 by reducing these temperature values by about 60–80 °C.

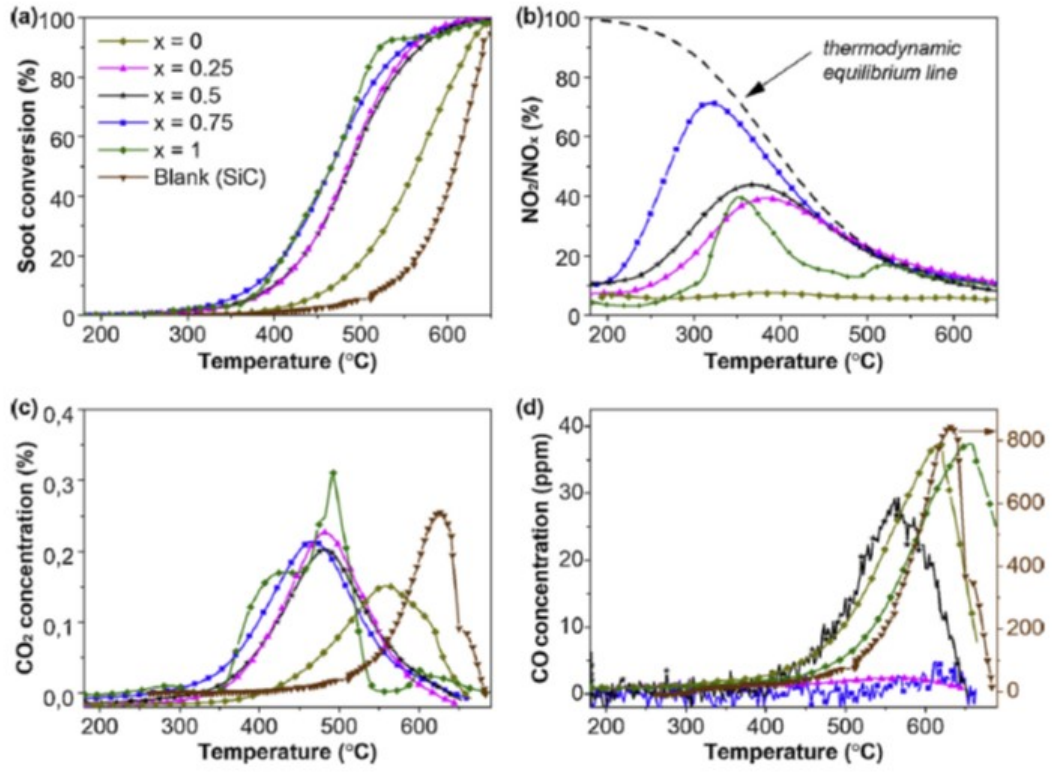

Fig. 9. (a) Soot conversion, (b) NO2 percentage, (c) CO2 and (d) CO concentrations of LaAl1-xCoxO3 calcined at 700 °C.

The improvement in the oxidation activity is likely to be related to not only the better performance in the NOx oxidation but also the NOx adsorption [35], as the Co doping reduces the NOx desorption temperature thereby facilitating the oxidation reactions at a lower temperature range (Fig. 6). As expected, both samples LaAl0.75Co0.25O3 and LaAl0.5Co0.5O3 (violet and black curves) exhibit similar soot oxidation activity, which is in line with the NOx-TPD experiments. This suggests that the NOx-assisted soot oxidation is mainly governed by the adsorption of NOx on the catalyst's surface and directed to the soot-catalyst interface before initiation of the oxidation [35]. LaAl0.25Co0.75O3 is the most active catalyst with T10% of 377 °C, which is 12 °C lower than that of LaCoO3. The complete substitution of Al by Co deteriorates the soot oxidation performance at low temperatures while there is no difference at middle temperature with T50% of 467 °C for both LaAl0.25Co0.75O3 and LaCoO3. The difference between these two catalysts is signified in terms of NO2 production which plays an essential role in abatement reduction. LaAl0.25Co0.75O3 maintains high formation of NO2 with NO2/NOx of 0.71 at 321 °C compared to 0.42 at 352 °C for LaCoO3. The low ignition temperature allows to uninterruptedly oxidize soot while keeping high NO2 production. In comparison with soot-free NO oxidation, NO2 production obtained from NOx-soot oxidation for all catalysts is lower, confirming the participation of NO2 as a strong oxidant in the reaction leading to its consumption.

LaAlO3 shows no formation of NO2 at all, explaining that the soot oxidation is practically the same as non-catalytic [86]. The outstanding performance of LaAl0.25Co0.75O3 is likely to be associated with the prominent lattice oxygen mobility which may be facilitated by coincorporation of Co-Al elements in perovskite structure [86,87]. Fig. 9c and d show the evolution of CO2 and CO concentration during the NOx-assisted oxidation tests over the catalysts with various Co content. Obviously, LaAlO3 has the highest Tmax (the temperature at which the maximum CO2 is produced) at 563 °C with low quantity of CO2 formed, evidenced by the CO2 selectivity of 82.3%. The substitution of Co by Al shifts the Tmax to lower range by about 81 °C for x=0.25 and 0.5, and by around 96 °C for LaAl0.25Co0.75O3. However, LaCoO3 shifts the temperature towards 493 °C which is similar to that reported elsewhere [27] and produces relatively a large amount of CO at high temperature. The CO2 evolution profile for LaCoO3 has a relatively similar trend as NO desorption curve with a broader shoulder at a low-temperature range (Fig. 6c), indicating the key role of NO adsorption on soot oxidation. When SiC was used as a reference for the non-catalytic soot oxidation, the promotional effect of NOx was lost as the peak of the soot oxidation rate was shifted to 626 °C coupled with a very high CO production.

Fig. 10 summarizes soot conversion and NO2/NOx percentage as functions of temperature over catalyst LaAl0.25Co0.75O3 calcined at different temperatures, and Table 9 sums up the oxidative characteristics of the catalyst. The calcination at lower temperatures enhances the surface areas but deteriorates the oxidation activity. The sample annealed at 500 °C has the highest T10%, T50% and T90% at 399, 492 and 583 °C respectively, compared to 370, 478 and 578 °C for LaAl0.25Co0.75O3 calcined at 600 °C. Moreover, the treatment at 600 and 700 °C shows similar soot oxidation but the NO2 production of the later is ameliorated with 71% compared to 64.9% for the former. It has been already mentioned that LaAl0.25Co0.75O3 calcined at the lowest temperature adsorbs the largest amount of NO due to high surface area but releases this gas at the highest temperature, suggesting that stronger interaction between NOx and substrate surface does not support the oxidation reaction and the products fail to dissociate as it can be described by the Sabatier principle [88]. This finding emphasizes the crucial role of crystallinity promoted by high calcination temperature in both NO and NOx-assisted soot oxidation.

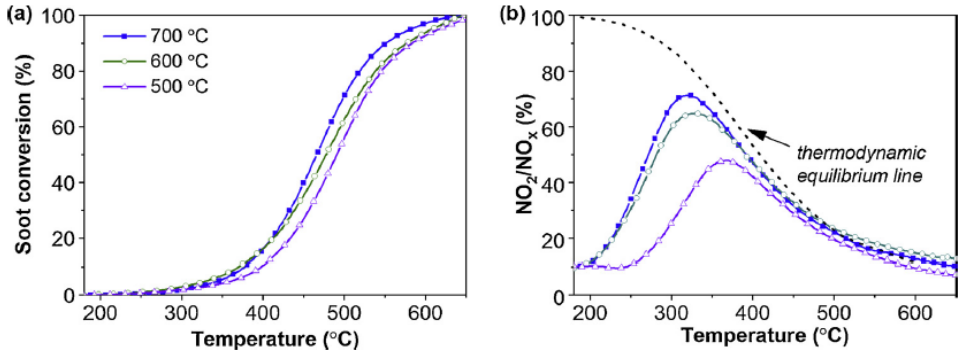

Fig. 10. (a) Soot oxidation and (b) NO2 percentage of aAl0.25Co0.75O3 calcined at different temperatures.

Calcination Temperature (°C)	$T_{10\%}$ (°C)	$T_{50\%}$ (°C)	T_{max} (°C)	$T_{90\%}$ (°C)	$(NO_2/NO_x)_{max}$ / T (%/°C)	CO_2 selectivity (%)
700	377	467	467	585	71.0 / 321	99.8
600	370	478	478	578	64.9 / 330	99.5
500	399	492	499	583	47.9 / 368	98.7

Table 9. Catalytic performances of LaAl0.25Co0.75O3 at different calcination temperatures.

4. Conclusions

Among the prepared catalysts, LaAl0.25Co0.75O3 exhibits superior catalytic activity for both NO oxidation and NOx-assisted soot oxidation. For the NO oxidation, NO2 production can reach 78% at relatively low temperature (320 °C) which is considered as a potential alternative for noble metal catalysts. Furthermore, LaAl0.25Co0.75O3 is also the most active catalyst for NOx-assisted soot oxidation with T10% of 377 °C and NO2/NOx of 0.71, and results in almost 100% of CO2 selectivity. The correlation between NOx desorption and oxidation activity is well established suggesting that NOx adsorption on catalyst surface is a key role in soot oxidation with NOx. The effect of NO2 for soot oxidation is obvious, since in its absence the oxidation activity remarkably decreases. The excellent performance of LaAl0.25Co0.75O3 is likely to be linked with high lattice surface oxygen supported by well-crystallized perovskite structure. Full replacement of Al by Co deteriorates the catalytic activity, suggesting that the combination of Al-Co has synergetic effects on the catalysis.

Acknowledgements

This work was co-funded through a SINCHEM Grant. SINCHEM (Sustainable Industrial Chemistry) is a Joint Doctorate programme selected under the Erasmus Mundus Action 1 Programme (FPA 2013-0037).

References

[1] M.A. Pena, J.L.G. Fierro, Chem. Rev. 101 (2001) 1981–2017.

[2] J. Zhu, H. Li, L. Zhong, P. Xiao, X. Xu, X. Yang, Z. Zhao, J. Li, ACS Catal. 4 (2014) 2917–2940.

[3] U. Oemar, P.S. Ang, K. Hidajat, S. Kawi, Int. J. Hydrogen Energy 38 (2013) 5525–5534.

[4] C.P.B. Quitete, R.L. Manfro, M.M.V.M. Souza, Int. J. Hydrogen Energy 42 (2017) 9873–9880.

[5] Yasushi, D. Mukai, Y. Murai, S. Tochiya, Y. Izutsu, K. Sekiguchi, N. Hosomura, H. Arai, E. Kikuchi, Y. Sugiura, Appl. Catal. A Gen. 451 (2013) 160–167.

[6] K.H. Lin, C. Bin Wang, S.H. Chien, Int. J. Hydrogen Energy 38 (2013) 3226–3232.

[7] Q. Zhang, L. Li, B. Jiang, K. Wang, D. Tang, B. Dou, Int. J. Hydrogen Energy 42 (2017) 17102–17111.

[8] K. Zhao, F. He, Z. Huang, G. Wei, A. Zheng, H. Li, Z. Zhao, Appl. Energy 168 (2016) 193–203.

[9] L.D. Vella, J.A. Villoria, S. Specchia, N. Mota, J.L.G. Fierro, V. Specchia, Catal. Today 171 (2011) 84–96.

[10] T.H. Nguyen, A. Łamacz, P. Beaunier, S. Czajkowska, M. Domański, A. Krztoń, T. Van Le, G. Djéga-Mariadassou, Appl. Catal. B Environ 152–153 (2014) 360–369.

[11] S. Ramesh, N.J. Venkatesha, ACS Sustan. Chem. Eng. 5 (2017) 1339–1346.

[12] J. Yao, J. Liu, H. Hofbauer, G. Chen, B. Yan, R. Shan, W. Li, Energy Convers. Manage. 117 (2016) 343–350.

[13] G. Chen, J. Yao, J. Liu, B. Yan, R. Shan, W. Li, Bioresour. Technol. 198 (2015) 108–114.

[14] G. Chen, J. Yao, J. Liu, B. Yan, R. Shan, Renew. Energy 91 (2016) 315–322.

[15] K.A. Resende, C.N. Vila-Neto, R.C. Rabelo-Neto, F.B. Noronha, C.E. Hori, Catal. Today 242 (2015) 71–79.

[16] X. Yang, L. Yang, W. Fan, H. Lin, Catal. Today 269 (2016) 56–64.

[17] M.-Y. Chen, C.-B. Chen, B. Zada, Y. Fu, M.H. Qiao, K.N. Fan, X.X. Zhang, B.N. Zong, A. Sarkar, M.K. Nazeeruddin, M. Grätzel, S.I. Seok, Green Chem. 18 (2016) 3858–3866.

[18] H. Deng, L. Lin, Y. Sun, C. Pang, J. Zhuang, P. Ouyang, Z. Li, S. Liu, Catal. Lett. 126 (2008) 106–111.

[19] H. Deng, L. Lin, Y. Sun, C. Pang, J. Zhuang, P. Ouyang, J. Li, S. Liu, Energy Fuels 23 (2009) 19–24.

[20] J.A. Onrubia, J.R. González-velasco, Appl. Catal. B Environ. 213 (2017) 198–210.

[21] X. Yang, L. Luo, H. Zhong, Catal. Commun. 6 (2005) 13–17.

[22] A.K. Ladavos, P.J. Pomonis, Appl. Catal. A Gen. 165 (1997) 73–85.

[23] N. Russo, S. Furfori, D. Fino, G. Saracco, V. Specchia, Appl. Catal. B Environ. 83 (2008) 85–95.

[24] S. Irusta, M.P. Pina, M. Men, J. Catal. 412 (1998) 400–412.

[25] A. Russell, W.S. Epling, Catal. Rev. - Sci. Eng. 53 (2011) 337–423.

[26] A. Namdeo, M.C. Bell, Environ. Int. 31 (2005) 565–573.

[27] R. Zhang, N. Luo, B. Chen, S. Kaliaguine, Energy Fuels 24 (2010) 3719–3726.

[28] T. Andana, M. Piumetti, S. Bensaid, L. Veyre, C. Thieuleux, N. Russo, D. Fino, E. Alessandra, R. Pirone, Appl. Catal. B Environ. 209 (2017) 295–310.

[29] E. Xue, K. Seshan, J.R.H. Ross, Appl. Catal. B Environ. 11 (1996) 65–79.

[30] M.V. Twigg, Catal. Today 117 (2006) 407–418.

[31] A. Setiabudi, M. Makkee, J.A. Moulijn, Appl. Catal. B Environ. 50 (2004) 185–194.

[32] M. Koebel, M. Elsener, M. Kleemann, Catal. Today 59 (2000) 335–345.

[33] M. Koebel, G. Madia, M. Elsener, Catal. Today 73 (2002) 239–247.

[34] M.K. Majewski, W.A. Khair, Diesel Emiss. Their Control. SAE Int., Warrendale, PA, 2006.

[35] T. Andana, M. Piumetti, S. Bensaid, L. Veyre, C. Thieuleux, N. Russo, D. Fino, E.A. Quadrelli, R. Pirone, Appl. Catal. B Environ. 226 (2018) 147–161.

[36] S. Liu, X. Wu, H. Luo, D. Weng, R. Ran, J. Phys. Chem. C 119 (2015) 17218–17227.

[37] H. Zhang, Y. Zhu, S. Wang, M. Zhao, M. Gong, Y. Chen, Fuel Process. Technol. J. 137 (2015) 38–47.

[38] S. Liu, X. Wu, D. Weng, M. Li, R. Ran, ACS Catal. 5 (2015) 909–919.

[39] C.H. Kim, G. Qi, K. Dahlberg, W. Li, Science (80-) 327 (2010) 1624–1627.

[40] J. Wang, Y. Su, X. Wang, J. Chen, Z. Zhao, M. Shen, Catal. Commun. 25 (2012) 106–106.

[41] V. Torregrosa-Rivero, V. Albaladejo-Fuentes, M.S. Sanchez-Adsuar, M.J. Illan-Gomez, RSC Adv. Open 7 (2017) 35228–35238.

[42] V.G. Milt, M.A. Ulla, E.E. Miro, Appl. Catal. B Environ. 57 (57) (2005) 13–21.

[43] N.T, P.V. Xin-Gang Li, Yan-Hua Dong, Hui Xian, Willinton Yesid Hernandez, Ming Meng, Hong-Hu Zou, Ai-Jing Ma, Tian-Yong Zhang, Zheng Jiang, Energy Environ. Sci. 4 (2011) 3351–3354.

[44] J. Chen, M. Shen, X. Wang, J. Wang, Y. Su, Z. Zhao, Catal. Commun. 37 (2013) 105–108.

[45] F. Lin, X. Wu, S. Liu, D. Weng, Y. Huang, Chem. Eng. J. 226 (2013) 105–112.

[46] T.R. Sahoo, M. Armandi, R. Arletti, M. Piumetti, S. Bensaid, M. Manzoli, S.R. Panda, B. Bonelli, Appl. Catal. B Environ. 211 (2017) 31–45.

[47] H. Lehnert, H. Boysen, J. Schneider, F. Frey, D. Hohlwein, P. Radaelli, H. Ehrenberg, Z. Kristallogr. Cryst. Mater. 215 (2000) 536.

[48] C.J. Howard, B.J. Kennedy, B.C. Chakoumakos, J. Phys. Condens. Matter 12 (2000) 349–365.

[49] G. Thornton, B.C. Tofield, A.W. Hewat, J. Solid State Chem. 61 (1986) 301–307.

[50] V. Aswin, P. Kumar, P. Singh, A. Gupta, S. Rayaprol, A. Dogra, J. Mater. Sci. 50 (2015) 366–373.

[51] R.D. Shannon, Acta Cryst (1976) 751.

[52] X. Zhu, X. Tu, M. Chen, Y. Yang, C. Zheng, J. Zhou, X. Gao, Catal. Commun. 92 (2017) 35–39.

[53] N.A. Merino, B.P. Barbero, P. Ruiz, L.E. Cadús, J. Catal. 240 (2006) 245–257.

[54] J. Zhang, X. Weng, Z. Wu, Y. Liu, H. Wang, Appl. Catal. B Environ. 126 (2012) 231–238.

[55] S. Ivanova, A. Senyshyn, E. Zhecheva, K. Tenchev, V. Nikolov, R. Stoyanova, H. Fuess, J. Alloys Compd. 480 (2009) 279–285.

[56] N.A. Merino, B.P. Barbero, P. Grange, L.E. Cadús, J. Catal. 231 (2005) 232–244.

[57] B. Białobok, J. Trawczyński, W. Miśta, M. Zawadzki, Appl. Catal. B Environ. 72 (2007) 395–403.

[58] T. Nakamura, G. Petzow, L.J. Gauckler, Mater. Res. Bull. 14 (1979) 649–659.

[59] B. Levasseur, S. Kaliaguine, Appl. Catal. A Gen. 343 (2008) 29–38.

[60] L.B. Sis, G.P. Wirtz, S.C. Sorenson, J. Appl. Phys. 44 (1973) 5553.

[61] L. Huang, M. Bassir, S. Kaliaguine, Appl. Surf. Sci. 243 (2005) 360–375.

[62] O.O. James, S. Maity, J. Pet, Technol. Altern. Fuels 7 (2016) 1–12.

[63] R. Sarbajna, A.S. Devi, K. Purandhar, M.V. Suryanarayana, Int. J. Chemtech Res. 5 (2013) 2810–2820.

[64] R. Zhang, A. Villanueva, H. Alamdari, S. Kaliaguine, Appl. Catal. B Environ. 64 (2006) 220–233.

[65] R. Pereñíguez, J.L. Hueso, F. Gaillard, J.P. Holgado, A. Caballero, Catal. Lett. 142 (2012) 408–416.

[66] S. Royer, F. Bérubé, S. Kaliaguine, Appl. Catal. A Gen. 282 (2005) 273–284.

[67] J. Zhang, D. Tan, Q. Meng, X. Weng, Z. Wu, Appl. Catal. B, Environ. 172–173 (2015) 18–26.

[68] R.R. Solís, F.J. Rivas, O. Gimeno, Appl. Catal. B Environ. 200 (2017) 83–92.

[69] M. O'Connell, A. Norman, C. Hüttermann, M. Morris, Catal. Today 47 (1999) 123–132.

[70] C.A.F. Vaz, D. Prabhakaran, E.I. Altman, V.E. Henrich, Phys. Rev. B - Condens. Matter Mater. Phys. 80 (2009) 1–7.

[71] C.A. Chagas, F.S. Toniolo, R.N.S.H. Magalhães, M. Schmal, Int. J. Hydrogen Energy 37 (2012) 5022–5031.

[72] M.C. Biesinger, B.P. Payne, A.P. Grosvenor, L.W.M. Lau, A.R. Gerson, R.S.C. Smart, Appl. Surf. Sci. 257 (2011) 2717–2730.

[73] F. Fang, N. Feng, L. Wang, J. Meng, G. Liu, P. Zhao, P. Gao, J. Ding, Appl. Catal. B Environ. 236 (2018) 184–194.

[74] C. Lee, Y. Jeon, S. Hata, J. Park, R. Akiyoshi, H. Saito, Y. Teraoka, Y. Shul, H. Einaga, Appl. Catal. B Environ. 191 (2016) 157–164.

[75] X. He, M. Meng, J. He, Z. Zou, X. Li, Z. Li, Z. Jiang, Catal. Commun. 12 (2010) 165–168.

[76] R. You, Y. Zhang, D. Liu, M. Meng, Z. Jiang, S. Zhang, Y. Huang, Chem. Eng. J. 260 (2015) 357–367.

[77] S. Roy, A. Baiker, Chem. Rev. 109 (2009) 4054–4091.

[78] J. Liu, Z. Zhao, C. Xu, A. Duan, G. Jiang, J. Phys. Chem. C 112 (2008) 5930–5941.

[79] S. Mentus, D. Jelić, V. Grudić, J. Therm. Anal. Calorim. 90 (2007) 393–397.

[80] Y. Peng, W. Si, J. Luo, W. Su, H. Chang, J. Li, J. Hao, J. Crittenden, Environ. Sci. Technol. 50 (2016) 6442–6448.

[81] J. Chen, M. Shen, X. Wang, G. Qi, J. Wang, W. Li, Appl. Catal. B Environ. 134–135 (2013) 251–257.

[82] A.-J. Ma, S.Z. Wang, C. Liu, H. Xian, Q. Ding, L. Guo, M. Meng, Y.S. Tan, N. Tsubaki, J. Zhang, L.R. Zheng, X.G. Li, Appl. Catal. B Environ. 146 (2014) 24–34.

[83] J. Xiong, Q. Wu, X. Mei, J. Liu, Y. Wei, Z. Zhao, D. Wu, J. Li, ACS Catal. 8 (2018) 7915–7930.

[84] P. Ciambelli, S. Cimino, G. Lasorella, L. Lisi, S. De Rossi, M. Faticanti, G. Minelli, P. Porta, Appl. Catal. B Environ. 37 (2002) 231–241.

[85] K. Tikhomirov, O. Kröcher, M. Elsener, A. Wokaun, Appl. Catal. B Environ. 64 (2006) 72–78.

[86] N.D. Wasalathanthri, T.M. SantaMaria, D.A. Kriz, S.L. Dissanayake, C.H. Kuo, S. Biswas, S.L. Suib, Appl. Catal. B Environ. 201 (2017) 543–551.

[87] C.M. Marcos, V.T. Rivero, V.A. Fuentes, M.S.S. Adsuar, M.J.I. Gómez, Top. Catal. 0 (2018) 0.

[88] G. Rothenberg, Catalysis: Concepts and Green Applications, WILEY-VCH Verlag, 2008.